INORGANIC CHEMISTRY
FRONTIERS

RESEARCH ARTICLE

View Article Online
View Journal | View Issue

Cite this: *Inorg. Chem. Front.*, 2023, **10**, 3015

Design of a robust rod-packing scandium–organic framework for C_2H_x/CO_2 separation, CO_2 storage, and catalytic CO_2 cycloaddition†

Hong-Juan Lv, Shu-Cong Fan, Yu-Cheng Jiang, * Shu-Ni Li and Quan-Guo Zhai *

Received 18th February 2023,
Accepted 8th April 2023

DOI: 10.1039/d3qi00314k

rsc.li/frontiers-inorganic

The exploration of efficient CO_2 capture and conversion techniques is of great importance for global sustainable development. Herein, a novel bi-microporous Sc-MOF, named $[Sc_3(NTB)_2(CH_3COO)_3]$ (SNNU-616-Sc, NTB = nitrilotribenzoic acid), was successfully designed and utilized for CO_2 storage and catalytic conversion. The linear $[Sc_3(COO)_6]$ trinuclear clusters were linked by triple acetate anions into 1D chains, which were further extended by NTB linkers and interleaved to produce the 3D robust rod-packing Sc-MOF with two types of open channels of about 12 Å and 3.8 Å, respectively. Notably, the bare N atom from NTB ligands can not only act as active sites to adsorb CO_2 molecules, but also provide Lewis basic sites for the CO_2 fixation reaction. Together with the high framework stability and two types of microporous open channels, SNNU-616-Sc shows high adsorption selectivity to effectively separate CO_2 from CO_2–C_2H_x binary mixtures (C_2H_x = acetylene, C_2H_2; ethylene, C_2H_4; ethane, C_2H_6), and a CO_2 storage capacity of 30 mmol g^{-1} (273 K and 29 bar), which surpasses most MOF adsorbents. Moreover, SNNU-616-Sc can also serve as an efficient recyclable catalyst for CO_2 fixation with epoxides in the presence of tetrabutylammonium bromide as a co-catalyst without any organic solvent under mild conditions. Particularly, for the catalytic reaction of CO_2 cycloaddition with epoxide bromopropane, the yields of cyclic carbonates can reach up to 97.5% with the selectivity higher than 98% and a conversion of 99%.

Introduction

The greenhouse gas carbon dioxide is the main cause of global warming, and its excessive emissions caused by the combustion of fossil fuel can bring about a series of serious environmental issues, such as extreme weather, ocean acidification, and the greenhouse effect.[1,2] It is extremely critical to develop efficient technologies for the mitigation of CO_2 emission to tremendously reduce the energy crisis and concurrently diminish environmental issues.[3–5] In order to achieve this purpose, many contributions have been made by researchers in various fields in recent years.[6,7]

On the one hand, physical capture technology for CO_2 molecules using porous solid adsorbents and the selective separation of CO_2 from the C2-hydrocarbons produced from industrial manufacture[8–10] have attracted researchers' particular interest, as well as developing a series of materials for selective CO_2 capture and separation from C2-hydrocarbons (C_2H_2, C_2H_4 and C_2H_6).[11–18] On the other hand, to face environmental problems, converting CO_2 to value-added chemical products for CO_2 aftertreatment that can achieve a carbon-neutral energy cycle in the environment has also raised considerable concerns.[2,19] Considering that the multifunctional applications of cyclic carbonates, such as solvents, degreasers, electrolytes in lithium-ion batteries, and precursors for the synthesis of fine chemicals and various polycarbonates,[20,21] adding the excellent properties of stability and low toxic, the conversion of CO_2 into cyclic carbonate becoming the most promising strategies for CO_2 fixation.[22] However, it is challenging to develop efficient, economical, and recyclable heterogeneous catalysts for CO_2 conversion because of the high thermodynamic energy barrier for the inert C=O bond of CO_2 molecules. Summing up the above, developing a kind of efficient CO_2 capture and conversion technique with mild operating conditions and low energy consumption would decrease the global energy demand and carbon emission.

In recent decades, metal–organic frameworks (MOFs), a kind of promising crystalline porous material constructed

Key Laboratory of Macromolecular Science of Shaanxi Province, Key Laboratory of Applied Surface and Colloid Chemistry, Ministry of Education, School of Chemistry & Chemical Engineering, Shaanxi Normal University, Xi'an, Shaanxi, 710062, China. E-mail: jyc@snnu.edu.cn, zhaiqg@snnu.edu.cn

†Electronic supplementary information (ESI) available. CCDC 2242282. For ESI and crystallographic data in CIF or other electronic format see DOI: https://doi.org/10.1039/d3qi00314k

from functionally organic linkers coupled with metal ions/clusters, have drawn much attention due to their high specific surface area, excellent porosity, regular pore systems, good chemical stability, and various topologies.[23–31] Considering the exploitation of new absorbents, MOF materials are undoubtedly used as a candidate to ease the emission of greenhouse gases due to the advantages above and play important roles in catalyzing CO_2 cycloaddition with epoxides in the CO_2 fixation reaction.[32–34]

Given all this, a novel highly stable bi-microporous Sc-MOF (SNNU-616-Sc) with bare Lewis basic nitrogen sites was successfully synthesized to develop efficient CO_2 capture and conversion materials. Thanks to the synergistic effects of extra-stability, open N sites and bi-microporosity, SNNU-616-Sc exhibits top-level CO_2 storage capacity and efficient separation ability for the binary mixture of CO_2–C2-hydrocarbons. Moreover, 1D channels with a size of about 12 Å in this structure can improve the mass transfer rate of the substrate during the catalytic reaction, which makes the SNNU-616-Sc material an efficient recyclable catalyst for CO_2 fixation with epoxides. And the possible reaction mechanism for the catalytic reaction of CO_2 cycloaddition was also discussed.

Experimental section

Materials and methods

$Sc(NO_3)_3{\cdot}9H_2O$, nitrilotribenzoic acid (H_3NTB), *N*,*N*-dimethylformide (DMF), acetonitrile (CH_3CN), and acetic acid (CH_3COOH) were from commercial sources without further purification. Powder X-ray diffraction (PXRD) data were collected on a MiniFlex 600 X-ray diffractometer over the 2θ range of 5–50° using Cu Kα radiation at room temperature. Thermogravimetric analyses (TGA) were carried out in the range of 25–900 °C using an HCT-1 thermal analyzer with a heating rate of 2 °C min^{-1} under a N_2 atmosphere. The high pressure gas adsorption performance for CO_2 was analyzed on a BSD-PH high pressure gas sorption analyzer. Gas adsorption isotherms under 1 bar were obtained by using a 3-Flex surface-area and pore-size analyzer, and CO_2, C_2H_4, C_2H_2, C_2H_6 and N_2, and all gases used in the adsorption experiment were of 99.99% purity. Breakthrough experiments were conducted on a home-built dynamic gas breakthrough set-up.

Synthesis

Synthesis of $[Sc_3(NTB)_2(CH_3COO)_3]$ (SNNU-616-Sc). NTB (9 mg, 0.024 mmol) and $Sc(NO_3)_3{\cdot}9H_2O$ (11 mg, 0.048 mmol) were dissolved in a mixed solution of 2 mL DMF and 2 mL CH_3CN in a 25 mL glass vial, and then 0.5 mL of CH_3COOH were added to this solution and sealed. After sonication for 10 minutes, the raw materials were completely dissolved to obtain a clear solution, and then the vial was placed into the oven and heated to 120 °C for 6 days. After the temperature dropped to room temperature, yellowish block crystals of SNNU-616-Sc were obtained and washed with fresh DMF. The crystal photo of the optical microscope is shown in Fig. S1.†

X-Ray single crystal structure determination

The diffraction data of the single crystal sample for SNNU-616-Sc were collected using a Bruker APEX-II CCD with GaKα (λ = 1.34139) radiation at 170 K. The structure was solved and refined by direct methods using the SHELXS program. All non-hydrogen atoms were refined anisotropically. The detailed crystallographic data and the structure refinement parameters of SNNU-616-Sc are summarized in Table S1.† Selected bond lengths and bond angles are given in Table S2.†

Gas adsorption

Before the measurements of gas adsorption, samples were exchanged with fresh pentane solvent and vacuum heated at 393 K for 10 h to obtain activated MOF samples. In order to evaluate the permanent porosity of SNNU-616-Sc, N_2 adsorption measurements were conducted at 77 K. Gas adsorption measurements of activated samples for single components (CO_2, C_2H_4, C_2H_2, and C_2H_6) at different temperatures (273 K, 283 K, and 298 K) were performed to evaluate the feasibility of SNNU-616-Sc MOF as an adsorbent material to separate CO_2 from the CO_2–C_2H_x mixtures. High pressure gas adsorption performance analysis for CO_2 was conducted at different temperatures to evaluate the storage ability of SNNU-616-Sc.

Breakthrough experiments

To further verify the actual binary CO_2–C2-hydrocarbon separation performance, breakthrough column experiments were conducted for activated SNNU-616-Sc. About 500 mg of MOF samples were filled in a stainless-steel column (a length of 12 cm, an inner diameter of 0.44 cm, an external diameter of 0.6 cm), and helium was passed with the flow rate of 20 mL min^{-1} under ambient pressure at room temperature for 12 h to activate further. Subsequently, a CO_2–C_2H_x (50/50) mixture gas was passed into the column. Before each testing, a helium flow of 30 mL min^{-1} had to be maintained for 2–3 h to remove the air and residual gas molecule from the column.

Catalytic CO_2 cycloaddition

Before the catalytic trials, SNNU-616-Sc was activated at 393 K under high vacuum (10^{-6} Torr) for 10 h. The activated-MOF catalyst (20 mg), epoxide substrates (20 mmol), and nBu$_4$NBr (32 mg, 0.1 mmol) were placed in a Teflon sample holder inside a stainless-steel reactor. Before the catalytic reactions, the system was filled with CO_2 to get rid of the residual air and then the reactor was sealed and pressurized with CO_2 until 0.8 MPa, and the reactions proceeded at 80 °C for 8 h under stirring. After the catalytic reaction, the reactor was cooled in a water bath, and then ethyl acetate was added into the reactor and the product was taken out. The as-obtained suspension was finally centrifuged to obtain the liquid supernatant and diluted with ethyl acetate. After that, the product was analysed by gas chromatography with a flame ionization detector. For the recycling tests, the supernatant liquid was carefully removed after each catalytic run, and the solid catalyst was

washed with acetone and dried to remove all volatile compounds before reusing for further catalytic cycles.

Results and discussion

Structural analysis

Single crystal X-ray diffraction analysis revealed that SNNU-616-Sc crystallizes in the trigonal system, space group $R\bar{3}$. Each Sc(III) atom connects six O atoms to form an octahedral coordination model (Fig. 1a), and adjacent three Sc(III) atoms are linked by six carboxylates from six NTB organic linkers to afford a linear $[Sc_3(COO)_6]$ trinuclear cluster. As shown in Fig. 1b, each NTB ligand connects three linear trinuclear clusters. Each linear trinuclear motif is bridged by three acetate anions, generating a 1D metal–organic chain (Fig. 1d). Three neighbour 1D chains were further connected by NTB linkers (Fig. 1c) in different directions, and thus interleaved to produce the 3D architecture of SNNU-616-Sc (Fig. 1e and f). Notably, two types of 1D channels with different sizes are observed along the *c*-axis direction, which are larger hexagonal and smaller triangular channels with their sizes of about 12 Å and 3.8 Å, respectively (Fig. 1e). Furthermore, the 1D Sc-carboxylate chains can be regarded as rod-like secondary building units, which make SNNU-616-Sc a novel rod-packing metal–organic framework.

It is noted that the small pore with a size of 3.8 Å is obviously fitting for selective CO_2 adsorption (CO_2, 3.18 × 3.33 × 5.36 $Å^3$; C_2H_2, 3.32 × 3.34 × 5.7 $Å^3$; C_2H_4, 3.28 × 4.18 × 4.84 $Å^3$; C_2H_6, 4.08 × 3.81 × 4.82 $Å^3$).[35] Combined with the bare nitrogen atoms as efficient adsorptive sites for CO_2 molecules, SNNU-616-Sc should be a good candidate for CO_2 adsorption and separation applications under low pressure. The other pore of about 12 Å is large enough to facilitate not only high-pressure storage for CO_2, but also rapid diffusion of molecules inside the pores, which can be expected to offer a confined space to accelerate the mass transfer and facilitate the catalytic reaction. Clearly, SNNU-616-Sc has great potential as a tri-functional material for C_2H_x/CO_2 separation, CO_2 storage, and catalytic CO_2 fixation.

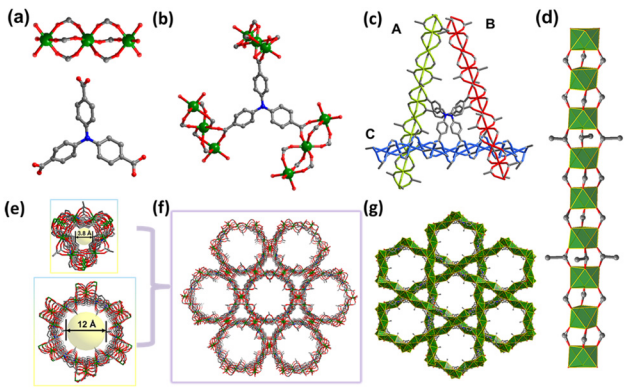

Fig. 1 The structures of SNNU-616-Sc: (a) the linear $[Sc_3(COO)_6]$ trinuclear cluster; (b) the linkage between $[Sc_3]$-clusters and the NTB ligand; (c) the distribution of three 1D chains from different directions; (d) the detailed structure of the 1D chain extended by acetate anions and $[Sc_3]$-clusters; (e) two types of 1D open channels with different sizes; (f) and (g) the 3D framework viewed along the *c*-axis direction.

Stability measurements and porosity characterization

The phase purity of the as-synthesized and activated SNNU-616-Sc MOF samples was confirmed by PXRD measurements (Fig. 2a). The chemical stability was measured by the treatment of MOF samples (30 mg) in solution (10 mL) with different pH values. The PXRD patterns of the as-synthesized and treated MOF samples matched well with the simulated pattern from the data of single crystal X-ray diffraction. These results indicated that SNNU-616-Sc can keep the skeleton intact for more than 48 h in the solutions with a wide pH value range from 3 to 11. The TGA curves (Fig. S2†) showed that the main temperature points of collapse for the SNNU-616-Sc sample before and after solvent exchange were similar. At the very beginning, the weight loss for the solvent-exchanged sample was observed below 373 K because of the loss of solvent molecules. After that, the skeleton was stable up to about 720 K under a N_2 atmosphere and the framework will collapse over this temperature, which confirms the high thermal stability of SNNU-616-Sc.

N_2 adsorption–desorption isotherms at 77 K confirmed that SNNU-616-Sc has excellent textural properties and exhibits permanent microporosity, as evidenced by reversible type I adsorption isotherms (Fig. 2b). The pore size distributions (PSD) determined by non-local density functional theory (NLDFT) are presented in Fig. 2b (inset). Two main types of pore sizes are observed, which are basically in accordance with the results indicated by the single crystal structure. Moreover, the Brunauer–Emmett–Teller specific surface area calculated from N_2 adsorption isotherms is 1398 $m^2\ g^{-1}$ and the pore volume is 0.87 $cm^3\ g^{-1}$ for SNNU-616-Sc, which further indicate the great adsorption ability because the adsorption ability of the materials for CO_2 largely depends on the specific surface area and the micropore volume of the adsorbent.[36] In comparison to the reported MOF materials, the BET surface area of SNNU-616-Sc is less than those of MOF-177 (4508 $m^2\ g^{-1}$),[37] ZJU-195a (1722 $m^2\ g^{-1}$),[38] and MOF-505 (1547 $m^2\ g^{-1}$),[37] and but higher than those of many famous reported MOF materials, such as MIL-53 (Cr) (1197 $m^2\ g^{-1}$),[39] UPC-110

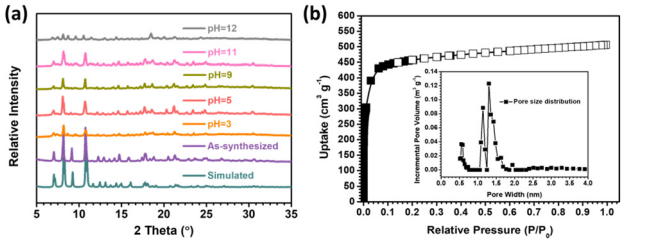

Fig. 2 (a) PXRD patterns for SNNU-616-Sc after different treatments; (b) N_2 adsorption–desorption isotherms at 77 K and the pore size distributions for SNNU-616-Sc.

(1384 m^2 g^{-1}),[40] SNNU-45 (1007 m^2 g^{-1}),[41] and NKMOF-1-Ni (382 m^2 g^{-1}).[42]

Gas adsorption

The single-component gas adsorption experiments for CO_2, C_2H_4, C_2H_2, and C_2H_6 were first conducted at different temperatures to explore the CO_2 adsorption and separation performance for SNNU-616-Sc. According to Fig. 3, the CO_2 uptake is 36.3 cm^3 g^{-1} at 298 K and 1.0 bar. Under the same conditions, these values for C_2H_4, C_2H_2, and C_2H_6 are 69.6, 76.3, and 77.7 cm^3 g^{-1}, respectively. Obviously, SNNU-616-Sc shows much higher uptake capacity for C2-hydrocarbons than for CO_2. In addition, the steeper adsorption curves of C_2H_4, C_2H_2, and C_2H_6 in the range of low pressure were reflected in a wide range of temperatures from 273 K to 298 K, which indicate stronger interactions with the MOF skeleton and indicate great potential for the separation of CO_2 molecules from the C2-hydrocarbons.

The adsorption heat (Q_{st}) in SNNU-616-Sc was further calculated based on the virial equations (eqn (S1) and (S2)†) to evaluate the binding strength between the MOF and gas molecules. The value of adsorption heat for CO_2 at zero-coverage (20.3 kJ mol^{-1}) is much lower than the values of C_2H_4 (27 kJ mol^{-1}), C_2H_2 (28.7 kJ mol^{-1}), and C_2H_6 (27.5 kJ mol^{-1}) (Fig. 4a and S3†). These results indicate stronger interactions with the MOF skeleton for C_2H_x than CO_2 molecules, which are line with the adsorption curves under lower pressure. In addition, the $-Q_{st}$ value at zero-coverage of CO_2 is less than those of many best CO_2-uptake MOFs such as UTSA-74a (25 kJ mol^{-1}),[43] NKMOF-1-Ni (40.9 kJ mol^{-1}),[42] JCM-1 (33.4 kJ mol^{-1}),[44] and JXNU-5 (25.2 kJ mol^{-1}),[45] indicating the low regenerative energy consumption of SNNU-616-Sc during the process of recycling.

The ideal adsorbed solution theory (IAST) was applied to calculate the separation performance for binary CO_2–C_2H_x mixtures. The adsorption isotherms at 298 K were fitted by the

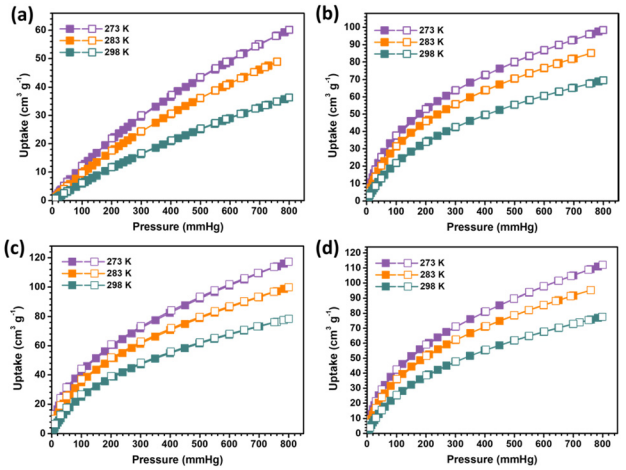

Fig. 3 The gas adsorption isotherms at different temperatures: (a) CO_2; (b) C_2H_4; (c) C_2H_2; and (d) C_2H_6.

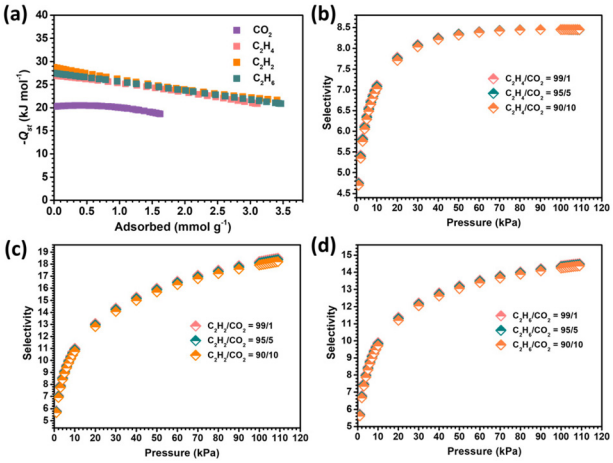

Fig. 4 The calculated adsorption enthalpy for different gases (a), and the IAST separation selectivity at 298 K in SNNU-616-Sc for C_2H_4/CO_2 (b), C_2H_2/CO_2 (c), and C_2H_6/CO_2 (d).

Langmuir–Freundlich equation (eqn (S3)†). As shown in Fig. S4,† the calculated equimolar mixed gas selectivity values of C_2H_4/CO_2, C_2H_2/CO_2, and C_2H_6/CO_2 at 298 K and 1.0 bar are 8.4, 16.5, and 13.5, respectively. The C_2H_x/CO_2 separation ability for different components at 298 K was further calculated (Fig. 4b–d), which shows that with the increase of pressure, the selectivity values increase. This can be attributed to the lateral interactions between CO_2 molecules that were enhanced as the mixture pressure increased.[46] Particularly, one percent of CO_2 in the binary mixture of C_2H_x/CO_2 still show good separation selectivity, indicating the excellent ability of removing trace CO_2 from the CO_2–C_2H_x mixtures. In general, SNNU-616-Sc has good separation potential to remove CO_2 from the binary mixture of CO_2–C2-hydrocarbons.

Breakthrough experiments

To confirm the practical separation performance of SNNU-616-Sc for the CO_2–C_2H_x mixture, breakthrough experiments were conducted. The binary mixture of CO_2–C_2H_x was injected into a packed column with a flow rate of 2.0 mL min^{-1} at 298 K to evaluate the separation performance. As depicted in Fig. 5a, the CO_2 molecule broke through the bed quickly after feeding the gas mixture into the fixed adsorption column, while the detection time for C_2H_4, C_2H_2, and C_2H_6 is later than that of CO_2 for these three kinds of binary mixtures, showing that the component of C2-hydrocarbons can remain for a longer time in comparison to the CO_2 molecules in the breakthrough column. According to the breakthrough curves, CO_2 molecules broke through the column at a time of 14.7 min g^{-1}, whereas the time for C_2H_4, C_2H_2, and C_2H_6 was retained in the adsorption bed for 32.7, 31.6, and 34.9 min g^{-1}, respectively, which indicate the stronger interaction between C2-hydrocarbons and the skeleton of SNNU-616-Sc than that of CO_2, in line with the results of adsorption enthalpy. And the breakthrough time gaps for these three kinds of binary mixtures (C_2H_4/CO_2, C_2H_2/CO_2, C_2H_6/CO_2) are similar to each other, which indicate an

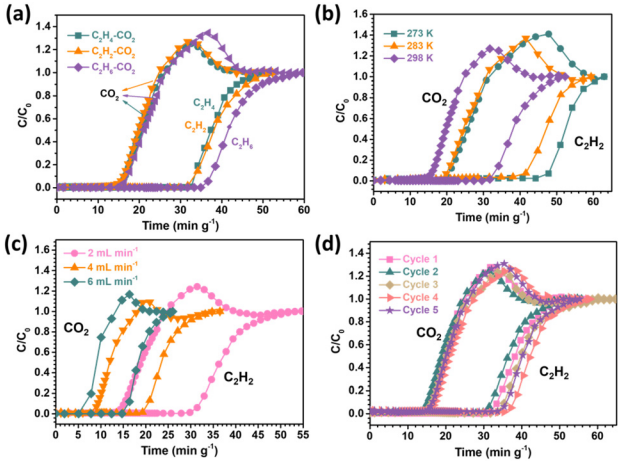

Fig. 5 Breakthrough curves of SNNU-616-Sc under 1 bar for three equimolar mixtures at 298 K with the flow rate of 2 mL min^{-1} (a), the C_2H_2/CO_2 mixture at different temperatures with a flow rate of 2 mL min^{-1} (b), the C_2H_2/CO_2 mixture with different flow rates at 298 K (c), and five recycling breakthrough curves for C_2H_2/CO_2 at 298 K with a flow rate of 2 mL min^{-1} (d).

excellent separation performance based on the porous absorbent material SNNU-616-Sc. The actual capture amount of four kinds of gases calculated from the breakthrough curves (eqn (S5) and (S6)†) was 0.89, 1.7, 1.75, and 1.9 mmol g^{-1} for CO_2, C_2H_4, C_2H_2, and C_2H_6, respectively. And the separation factors for C_2H_4/CO_2, C_2H_2/CO_2, and C_2H_6/CO_2 were 1.91, 1.97 and 2.13. Moreover, the purity of the obtained CO_2 from the three mixtures is above 99.5%.

Moreover, the breakthrough experiments of the C_2H_2/CO_2 binary mixture under different conditions were further conducted to explore the effects of temperature and gas flow rate on the separation performance in actual application. As shown in Fig. 5b, the separation interval time of SNNU-616-Sc for C_2H_2/CO_2 is 15.8 min g^{-1} at 298 K and 1 bar, which increases with the decreasing temperature. The separation time is shorter than that of reported materials such as JCM-1,[44] UTSA-74a,[47] and FJU-90a,[48] and comparable to the benchmark ZJUT-2a,[49] and UPC-200(Al)-F-BIM.[50] At 283 K and 273 K, the separation interval times reach 21.2 min g^{-1} and 25.4 min g^{-1}, respectively. On the other hand, when the flow rate decreases, the separation interval time increases clearly, but when the gas flow rate increases, a shorter separation interval time and smaller transfer mass were observed (Fig. 5c). Even with a flow rate of 6 mL min^{-1}, the C_2H_2/CO_2 separation interval time still is about 10 min g^{-1}.

Ideal gas adsorbents should have good recyclability in practical industrial applications. Five successive C_2H_2/CO_2 dynamic breakthrough experiments were carried out on SNNU-616-Sc at 298 K and 1 bar with a flow rate of 2 mL min^{-1} to evaluate the recyclability. As shown in Fig. 5d, almost constant breakthrough curves indicate its outstanding recyclability and stability. Furthermore, the breakthrough curves at different temperatures for C_2H_4/CO_2 and C_2H_6/CO_2 were also

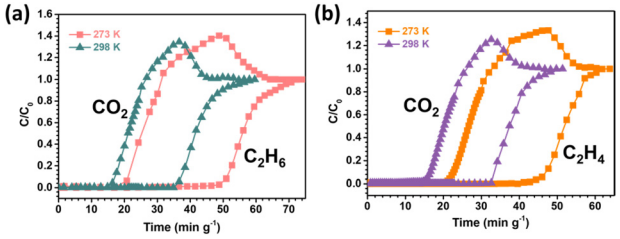

Fig. 6 The breakthrough curves at different temperatures under 1 bar with the flow rate of 2 mL min^{-1} for C_2H_6/CO_2 (a) and C_2H_4/CO_2 (b).

evaluated and are depicted in Fig. 6. Similar to the C_2H_2/CO_2 mixture, the separation interval time increases to about 30 and 25 min g^{-1} for C_2H_6/CO_2 and C_2H_4/CO_2 mixtures at 273 K. In our opinion, the smaller triangular channels with a size of 3.8 Å in the structure of Sc-MOF should mainly contribute to the prominent C_2H_x/CO_2 separation performance, which surpasses many famous MOF adsorbents and makes SNNU-616-Sc a great adsorbent for practical separation in industrial applications.

High-pressure CO_2 storage

The single-component CO_2 adsorption isotherm of SNNU-616-Sc has no tendency of gentle curve in comparison to the other three C2-hydrocarbon gases from 0 to 1 bar, which indicates that SNNU-616-Sc may be can adsorb much more CO_2 under higher pressure. At the same time, taking the high BET specific surface area (1398 m^2 g^{-1}) and larger pore size of 1D hexagonal channels (12 Å) into account, SNNU-616-Sc should be more propitious to high-pressure CO_2 storage. High-pressure CO_2 adsorption results at different temperatures for SNNU-616-Sc show that the storage capacity can reach as high as 30 mmol g^{-1} (672.2 cm^3 g^{-1} and 48.8 wt%) at 273 K and 29 bar (Fig. 7a and Table S4†), which is slightly lower than the performance of MFM-160a (32 mmol g^{-1}, 19.8 bar) and superior to most MOFs reported at 273 K (Fig. S7†), such as MIL-125-Ti (10.761 mmol g^{-1}, 9.8 bar),[51] β-Zn (8 mmol g^{-1}, 28 bar),[52] MIX-MIL-125-Ti (7.71 mmol g^{-1}, 9.8 bar),[51] MOF-74-Mg (~7 mmol g^{-1}, 30 bar),[53] MFC-1 (6.7 mmol g^{-1}, 30 bar),[53] MIL-100-Fe (0.62 mmol g^{-1}, 30 bar),[53] and MMC1 (~0.6 mmol g^{-1}, 30 bar).[53] At room temperature, SNNU-616-Sc still can take up CO_2 of 17.1 mmol g^{-1} (384.3 cm^3 g^{-1}, 29 bar), which was competitive with many famous MOFs under the same con-

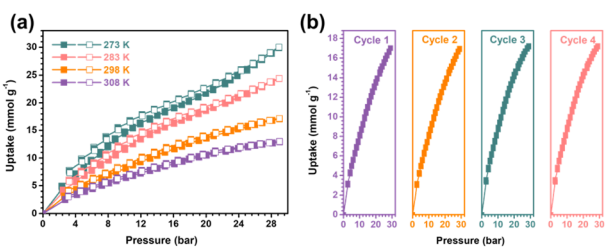

Fig. 7 The high-pressure CO_2 adsorption–desorption curves at different temperatures (a) and the recyclability results (b) at 298 K.

ditions like MOF-505 (18 mmol g^{-1}, 30 bar),[37] MIL-101-Cr (14.38 mmol g^{-1}, 40 bar),[54] MIL-53-Cr (10.6 mmol g^{-1}, 25 bar),[39] and MIL-53-Al (9.5 mmol g^{-1}, 25 bar).[55] Besides, SNNU-616-Sc displays excellent reusability for CO_2 storage under at least five regeneration conditions (Fig. 7b).

GCMC simulations

GCMC simulations were further adopted for SNNU-616-Sc to investigate the probable adsorption sites of CO_2 and C2-hydrocarbons in the MOF skeleton. As shown in Fig. S8,† the probable sites of CO_2 molecules in SNNU-616-Sc are mainly distributed in triangular channels with a suitable pore size, and the second sites are distributed in the surroundings of the N atom sites from the NTB ligands. SNNU-616-Sc shows three same binding site distribution toward C_2H_2, C_2H_4, and C_2H_6, in which the first two adsorptive sites are the same as for CO_2 molecules. The third sites are within the larger hexagonal channels. So, the number of adsorptive sites for C2-hydrocarbons is clearly more than those for CO_2 molecules in the structure of SNNU-616-Sc, combined with the suitable pore volume and the higher strength of the interaction between C2 hydrocarbons and the skeleton than the CO_2 molecules, and further supports the efficient separation performance of CO_2 molecules from C_2H_x/CO_2 mixtures.

The difference in the interactions between guest molecules and the MOF skeleton in the SNNU-616-Sc may arise from the Lewis basic bare N sites. The binding sites of CO_2, C_2H_4, C_2H_2 and C_2H_6 were further evaluated by modelling studies. The distances of C–H···N for C2-hydrocarbons (C_2H_4, C_2H_2, and C_2H_6) and O=C···N for CO_2 molecules were obtained. As given in Fig. 8, the O=C···N distance for CO_2 molecules (5.05 Å) is markedly longer than the C–H···N distances for C2-hydrocarbons (C_2H_4, 4.4 Å; C_2H_2, 4.98 Å; C_2H_6, 4.19 Å), showing stronger interactions of C2-hydrocarbons than CO_2, which also offers theoretic support for the effective CO_2–C2-hydrocarbon separation performance.

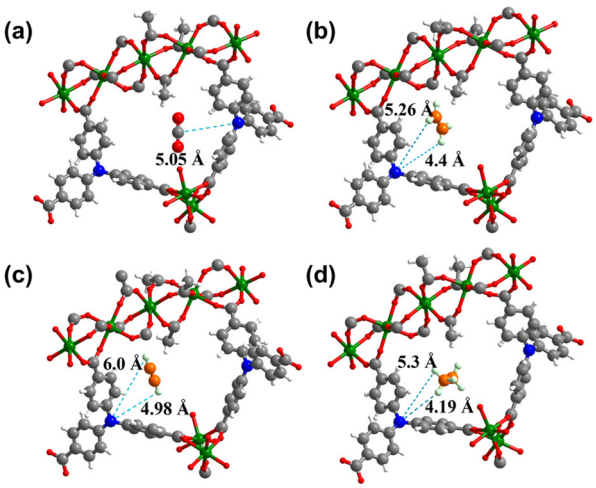

Fig. 8 The binding sites between bare N sites and CO_2 (a), C_2H_4 (b), C_2H_2 (c) and C_2H_6 (d) molecules calculated by modelling studies for SNNU-616-Sc.

Cycloaddition of CO_2 with epoxides

The prominent CO_2 adsorption and separation performances of SNNU-616-Sc encourage us to further investigate the catalytic activity for cycloaddition of epoxides with CO_2. Accordingly, a series of epoxide substrates were examined for the synthesis of the corresponding cyclic carbonates in the presence of SNNU-616-Sc as a catalyst at 0.8 MPa CO_2 pressure and 353 K (Table 1). As for entry 1 to entry 3, epoxides with alkyl chains of different lengths were used as substrates for the reaction, and the yields of epoxypropane, epoxybutane, and epoxy hexane were 95.8%, 94.2%, and 73.6%, respectively. Among them, epoxy hexane with the longest alkyl chain showed the lowest yield, which indicated that the catalyst activity of the cycloaddition reaction declined with the increase of steric hindrance. So, the effective size of the epoxides is necessary to facilitate their entrance into the channel to close the catalytically active sites. Only 74.6% of epoxy hexane was converted due to its difficult diffusion into the pores of the catalyst, and the difficulty of ring opening due to the large steric hindrance of the benzene ring hindering the Br^- attack also resulted in its low conversion. Moreover, SNNU-616-Sc exhibits highly efficient catalytic activity with a yield of 97.5% in carbonate formation after 8 h with 99% conversion and 98.6% selectivity when epoxide bromopropane was used as a reactant in the presence of nBu$_4$NBr as a co-catalyst (Table 1, entry 5).

The blank experiment (entry 6) by only adding the cocatalyst nBu$_4$NBr was conducted under the same conditions without SNNU-616-Sc, and the yield of cyclic carbonates is only

Table 1 Catalytic performance of SNNU-616-Sc for the CO_2 cycloaddition reaction with different epoxides

No	Substrate	PCO_2 (MPa)	T (°C)	t (h)	Yield (%)	Con. (%)	Select. (%)
1		0.8	80	8	95.8	97.2	95.6
2		0.8	80	8	94.2	99.9	94.3
3	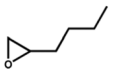	0.8	80	8	73.6	74.6	94.2
4		0.8	80	8	90.2	92.3	97.7
5		0.8	80	8	97.5	99	98.6
6[a]		0.8	80	8	52.5	47.5	98.8
7[b]		0.8	80	8	74.0	81.9	90.4
8[c]		0.8	80	8	37.7	36.7	99.8

Reaction conditions: epoxide = 20 mmol; catalyst = 20 mg SNNU-616-Sc; nBu$_4$NBr = 0.1 mmol, 32 mg; semi-batch reaction; determined by GC. [a] Without a catalyst. [b] Catalyst = $Sc(NO_3)_3{\cdot}9H_2O$. [c] Catalyst = NTB ligand.

52.5% with a low conversion rate of 47.5%, indicating that nBu$_4$NBr played an important role in ring opening, but it is deemed insufficient in improving the catalytic activity due to the lack of sufficient catalytic sites and mass transfer channels of the substrate. From the entries 5 and 6, Sc(NO$_3$)$_3$·9H$_2$O metal salts or NTB ligands are used as catalysts added to the reaction in the presence of nBu$_4$NBr, which shows clearly lower catalytic activity in comparison to the SNNU-616-Sc MOF catalyst. Therefore, the catalytic sites and mass transfer channels are of great significance in the catalytic reactions of CO_2 cycloaddition.

Recyclability is a critical criterion for an effective heterogeneous catalysis. The cycling experiments for epoxide bromopropane were also conducted under the same conditions (80 °C, 8 h, 0.8 MPa of CO_2 pressure) after easy separation and a simple filtration for SNNU-616-Sc, and washed several times with acetone. Fig. 9a shows that the recycled MOF catalyst can be reused up to at least five consecutive times without any considerable activity attenuation, showing an excellent recyclability. Moreover, the regenerative SNNU-616-Sc catalyst was analysed by PXRD. The PXRD patterns for the fresh MOF and recovered catalyst after 5 cycles are in full agreement with each other, further supporting the extraordinary catalytic stability of the SNNU-616-Sc catalyst (Fig. 9b).

Temperature-programmed desorption (TPD) of CO_2 and NH_3 analysis were performed to investigate the acid–base nature of the catalyst. As shown in Fig. S9,† SNNU-616-Sc shows an obvious peak at about 523 K for TPD-CO_2, and TPD-NH_3 has very little peaks over the whole range of temperatures, indicating the presence of strong basic sites in this structure and almost no acidic sites in the catalyst. The results of TPD analyses confirmed that the SNNU-616-Sc catalyst offers strong basic sites for the CO_2 cycloaddition catalytic reactions.

Cycloaddition reaction mechanism

Based on the single crystal structure, CO_2 adsorption and catalytic CO_2 cycloaddition of SNNU-616-Sc with epoxides, a plausible catalytic reaction mechanism was proposed.[56] As shown in Fig. 10, in the first step, the bare N sites with lone pair electrons acted as Lewis basic sites to activate CO_2 molecules. In the second step, Br^- anions generated from the co-catalyst

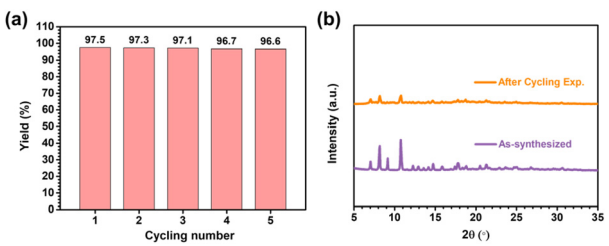

Fig. 9 (a) The yield of epoxide bromopropane for five catalytic cycles; (b) PXRD patterns for SNNU-616-Sc samples after the CO_2 cycloaddition reactions.

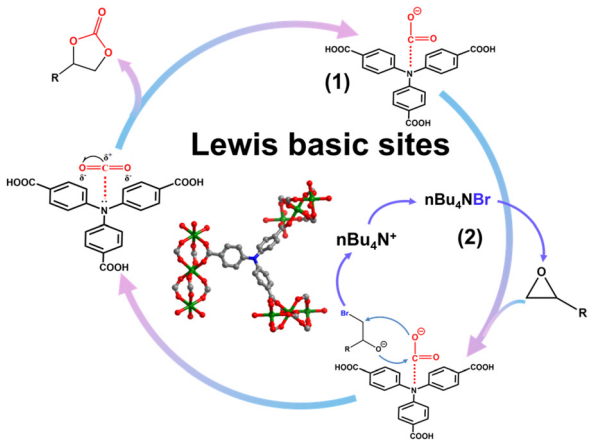

Fig. 10 The proposed catalytic mechanism of SNNU-616-Sc for CO_2 cycloaddition.

attack the less hindered C atom of the coordinated epoxides, followed by a ring-opening step. Thereafter, activated CO_2 interacts with the oxygen anion of the opened epoxy ring, forming an alkyl carbonate anion, and the corresponding cyclic carbonate is generated through ring closure with the elimination of the bromide ion. So, the good catalytic performance of SNNU-616-Sc is believed to be attributed to the synergistic effect of the basic catalytic sites and large mass transfer 1D channels in the presence of nBu$_4$NBr.

Conclusions

In this work, a robust rod-packing Sc-MOF with two types of micropores and Lewis basic bare N atoms was synthesized and utilized for CO_2 adsorption and conversion. Benefitting from the synergistic effects of high chemical and thermal stability, bi-microporous open channels, and bare N sites, the Sc-MOF exhibits not only a prominent separation ability of CO_2 from C_2H_x–CO_2 binary mixtures, but also an extra-high CO_2 storage capacity. Remarkably, the Sc-MOF also can act as an excellent catalyst for CO_2 cycloaddition with epoxides with high productivity, prominent selectivity, and good recyclability. In general, we offer a helpful route to explore novel CCS materials with high CO_2 adsorption and conversion performance under mild conditions, which are critical for the global energy demand and carbon emission.

Author contributions

Hong-Juan Lv: methodology, data collection and analysis, and writing the original draft. Shu-Cong Fan: investigation and data analysis. Yu-Cheng Jiang: formal analysis. Shu-Ni Li: investigation and resources. Quan-Guo Zhai: supervision, checking & editing, and funding acquisition.

Conflicts of interest

There are no conflicts to declare.

Acknowledgements

This work is financially supported by the National Natural Science Foundation of China (22071140), the Natural Science Foundation of Shaanxi Province (2021JLM-20), and the Fundamental Research Funds for the Central Universities (GK202101002).

References

1 D. Gilfillan and G. Marland, CDIAC-FF: Global and National CO_2 Emissions from Fossil Fuel Combustion and Cement Manufacture: 1751–2017, *Earth Syst. Sci. Data*, 2021, **13**, 1667–1680.
2 S. S. A. Shah, T. Najam, M. Wen, S.-Q. Zang, A. Waseem and H.-L. Jiang, Metal–Organic Framework-Based Electrocatalysts for CO2 Reduction, *Small Struct.*, 2022, **3**, 2100090.
3 J. Yu, L.-H. Xie, J.-R. Li, Y. Ma, J. M. Seminario and P. B. Balbuena, CO_2 Capture and Separations Using MOFs: Computational and Experimental Studies, *Chem. Rev.*, 2017, **117**, 9674–9754.
4 L. Lei, Y. Cheng, C. Chen, M. Kosari, Z. Jiang and C. He, Taming Structure and Modulating Carbon Dioxide (CO_2) Adsorption Isosteric Heat of Nickel-Based Metal Organic Framework (MOF-74(Ni)) for Remarkable CO_2 capture, *J. Colloid Interface Sci.*, 2022, **612**, 132–145.
5 Y. Ding, Z. Pang, K. Lan, Y. Yao, G. Panzarasa, L. Xu, M. Lo Ricco, D. R. Rammer, J. Y. Zhu, M. Hu, X. Pan, T. Li, I. Burgert and L. Hu, Emerging Engineered Wood for Building Applications, *Chem. Rev.*, 2023, **123**(5), 1843–1888.
6 F. A. Philip and A. Henni, Enhancement of Post-Combustion CO_2 Capture Capacity by Incorporation of Task-Specific Ionic Liquid into ZIF-8, *Microporous Mesoporous Mater.*, 2022, **330**, 111580.
7 D. Fu and M. E. Davis, Carbon Dioxide Capture with Zeotype Materials, *Chem. Soc. Rev.*, 2022, **51**, 9340–9370.
8 Y. Xie, H. Cui, H. Wu, R.-B. Lin, W. Zhou and B. Chen, Electrostatically Driven Selective Adsorption of Carbon Dioxide over Acetylene in an Ultramicroporous Material, *Angew. Chem., Int. Ed.*, 2021, **60**, 9604–9609.
9 Z. Zhang, S. B. Peh, R. Krishna, C. Kang, K. Chai, Y. Wang, D. Shi and D. Zhao, Optimal Pore Chemistry in an Ultramicroporous Metal-Organic Framework for Benchmark Inverse CO_2/C_2H_2 Separation, *Angew. Chem., Int. Ed.*, 2021, **60**, 17198–17204.
10 L. Jiao, J. Y. R. Seow, W. S. Skinner, Z. U. Wang and H.-L. Jiang, Metal–Organic Frameworks: Structures and Functional Applications, *Mater. Today*, 2019, **27**, 43–68.
11 Z. Zhu, J. Hu, X. Geng, B. Qin, K. Ma, Y. Wang and J. Gao, Process Design of Carbon Dioxide and Ethane Separation using Ionic Liquid by Extractive Distillation, *J. Chem. Technol. Biotechnol.*, 2018, **93**, 887–896.
12 H. Wang, M. Fan, Z. Zhang, J. Hao and C. Wang, Control of Cryogenic Extractive Distillation Process for Separating CO_2–C_2H_6 Azeotrope, *Comput. Chem. Eng.*, 2019, **128**, 384–391.
13 H. Wang, C. Wang, Z. Zhang, M. Fan, X. Yan and F. Li, Selection of State Equation and Innovative Process Design for Removing CO_2 by Azeotropic Distillation, *Chem. Eng. Technol.*, 2021, **44**, 710–722.
14 S. Wang, Q. Yang and C. Zhong, Adsorption and Separation of Binary Mixtures in a Metal-Organic Framework Cu-BTC: A Computational Study, *Sep. Purif. Technol.*, 2008, **60**, 30–35.
15 I. V. Zandvoort, E.-J. Ras, R. D. Graaf and R. Krishna, Using Transient Breakthrough Experiments for Screening of Adsorbents for Separation of C_2H_4/CO_2 Mixtures, *Sep. Purif. Technol.*, 2020, **241**, 116706.
16 G. Xu, Z. Meng, X. Guo, H. Zhu, K. Deng, C. Xiao and Y. Liu, Molecular Simulations on CO_2 Adsorption and Adsorptive Separation in Fullerene Impregnated MOF-177, MOF-180 and MOF-200, *Comput. Mater. Sci.*, 2019, **168**, 58–64.
17 H. J. Jun, D. K. Yoo and S. H. Jhung, Metal-organic Framework (MOF-808) Functionalized with Ethyleneamines: Selective Adsorbent to Capture CO_2 under Low Pressure, *J. CO2 Util.*, 2022, **58**, 101932.
18 Y. Wan, Y. Miao, R. Zhong and R. Zou, High-Selective CO_2 Capture in Amine-Decorated Al-MOFs, *Nanomaterials*, 2022, **12**, 4056–4065.
19 L. Wang, Y. Dong, T. Yan, Z. Hu, A. A. Jelle, D. M. Meira, P. N. Duchesne, J. Y. Y. Loh, C. Qiu, E. E. Storey, Y. Xu, W. Sun, M. Ghoussoub, N. P. Kherani, A. S. Helmy and G. A. Ozin, Black Indium Oxide a Photothermal CO_2 Hydrogenation Catalyst, *Nat. Commun.*, 2020, **11**, 2432.
20 T. Lescouet, C. Chizallet and D. Farrusseng, The Origin of the Activity of Amine-Functionalized Metal–Organic Frameworks in the Catalytic Synthesis of Cyclic Carbonates from Epoxide and CO_2, *ChemCatChem*, 2012, **4**, 1725–1728.
21 R. Babu, A. C. Kathalikkattil, R. Roshan, J. Tharun, D.-W. Kim and D.-W. Park, Dual-Porous Metal Organic Framework for Room Temperature CO_2 Fixation via Cyclic Carbonate Synthesis, *Green Chem.*, 2016, **18**, 232–242.
22 Y. Tang, W. Chen, R. Liu, L. Wang, Y. Pan, R. Bi, X. Feng, M. He, Q. Chen and Z. Zhang, Solvent-Free CO_2 Fixation Reaction Catalyzed by MOFs Composites Containing Polycarboxylic Acid Ligands, *ChemistrySelect*, 2021, **6**, 5350–5355.
23 Z. J. Chen, M. R. Mian, S. J. Lee, H. Y. Chen, X. Zhang, K. O. Kirlikovali, S. Shulda, P. Melix, A. S. Rosen, P. A. Parilla, T. Gennett, R. Q. Snurr, T. Islamoglu, T. Yildirim and O. K. Farha, Fine-Tuning a Robust Metal-Organic Framework toward Enhanced Clean Energy Gas Storage, *J. Am. Chem. Soc.*, 2021, **143**, 18838–18843.

24 J. Pei, X.-W. Gu, C.-C. Liang, B. Chen, B. Li and G. Qian, Robust and Radiation-Resistant Hofmann-Type Metal–Organic Frameworks for Record Xenon/Krypton Separation, *J. Am. Chem. Soc.*, 2022, **144**, 3200–3209.
25 L. Liu, S. Du, X. Guo, Y. Xiao, Z. Yin, N. Yang, Y. Bao, X. Zhu, S. Jin, Z. Feng and F. Zhang, Water-Stable Nickel Metal–Organic Framework Nanobelts for Cocatalyst-Free Photocatalytic Water Splitting to Produce Hydrogen, *J. Am. Chem. Soc.*, 2022, **144**, 2747–2754.
26 J.-D. Xiao and H.-L. Jiang, Metal–Organic Frameworks for Photocatalysis and Photothermal Catalysis, *Acc. Chem. Res.*, 2019, **52**, 356–366.
27 Y.-Y. Xue, X.-Y. Bai, J. Zhang, Y. Wang, S.-N. Li, Y.-C. Jiang, M.-C. Hu and Q.-G. Zhai, Precise Pore Space Partitions Combined with High-Density Hydrogen-Bonding Acceptors within Metal–Organic Frameworks for Highly Efficient Acetylene Storage and Separation, *Angew. Chem., Int. Ed.*, 2021, **60**, 10122–10128.
28 J. Wang, Y. Zhang, Y. Su, X. Liu, P. Zhang, R.-B. Lin, S. Chen, Q. Deng, Z. Zeng, S. Deng and B. Chen, Fine Pore Engineering in a Series of Isoreticular Metal-Organic Frameworks for Efficient C_2H_2/CO_2 separation, *Nat. Commun.*, 2022, **13**, 200.
29 X. Zhang, R.-B. Lin, H. Wu, Y. Huang, Y. Ye, J. Duan, W. Zhou, J.-R. Li and B. Chen, Maximizing Acetylene Packing Density for Highly Efficient C_2H_2/CO_2 Separation through Immobilization of Amine Sites within a Prototype MOF, *Chem. Eng. J.*, 2022, **431**, 134184.
30 X.-J. Kong and J.-R. Li, An Overview of Metal–Organic Frameworks for Green Chemical Engineering, *Engineering*, 2021, **7**, 1115–1139.
31 J.-R. Li, J. Yu, W. Lu, L.-B. Sun, J. Sculley, P. B. Balbuena and H.-C. Zhou, Porous Materials with Pre-Designed Single-Molecule Traps for CO_2 Selective Adsorption, *Nat. Commun.*, 2013, **4**, 1538.
32 B. Parmar, P. Patel, R. S. Pillai, R. K. Tak, R. I. Kureshy, N.-U. H. Khan and E. Suresh, Cycloaddition of CO_2 with an Epoxide-Bearing Oxindole Scaffold by a Metal–Organic Framework-Based Heterogeneous Catalyst under Ambient Conditions, *Inorg. Chem.*, 2019, **58**, 10084–10096.
33 G. Yunjang, C. Youngson and P. Dae-Won, Catalytic Performance of CPM-200-In/Mg in the Cycloaddition of CO_2 and Epoxides, *Catalysts*, 2021, **11**, 430–444.
34 S.-C. Fan, S.-Q. Chen, J.-W. Wang, Y.-P. Li, P. Zhang, Y. Wang, W. Yuan and Q.-G. Zhai, Precise Introduction of Single Vanadium Site into Indium–Organic Framework for CO_2 Capture and Photocatalytic Fixation, *Inorg. Chem.*, 2022, **61**, 14131–14139.
35 W. Xie, L. Yang, J. Zhang and X. Zhao, The Adsorptive Separation of Ethylene from C2 Hydrocarbons by Metal–Organic Frameworks, *Chem. – Eur. J.*, 2023, e202300158.
36 Y. Cao, Y. Zhao, Z. Lv, F. Song and Q. Zhong, Preparation and Enhanced CO_2 Adsorption Capacity of UiO-66/Graphene Oxide Composites, *J. Ind. Eng. Chem.*, 2015, **27**, 102–107.
37 A. R. Millward and O. M. Yaghi, Metal–Organic Frameworks with Exceptionally High Capacity for Storage of Carbon Dioxide at Room Temperature, *J. Am. Chem. Soc.*, 2005, **127**, 17998–17999.
38 L. Zhang, K. Jiang, Y. Li, D. Zhao, Y. Yang, Y. Cui, B. Chen and G. Qian, Microporous Metal–Organic Framework with Exposed Amino Functional Group for High Acetylene Storage and Excellent C_2H_2/CO_2 and C_2H_2/CH_4 Separations, *Cryst. Growth Des.*, 2017, **17**, 2319–2322.
39 X. Zhou, W. Huang, J. Liu, H. Wang and Z. Li, Quenched Breathing Effect, Enhanced CO_2 Uptake and Improved CO_2/CH_4 Selectivity of MIL-53(Cr)/Graphene Oxide Composites, *Chem. Eng. Sci.*, 2017, **167**, 98–104.
40 W. Fan, X. Wang, X. Liu, B. Xu, X. Zhang, W. Wang, X. Wang, Y. Wang, F. Dai, D. Yuan and D. Sun, Regulating C_2H_2 and CO_2 Storage and Separation through Pore Environment Modification in a Microporous Ni-MOF, *ACS Sustainable Chem. Eng.*, 2019, **7**, 2134–2140.
41 Y.-P. Li, Y. Wang, Y.-Y. Xue, H.-P. Li, Q.-G. Zhai, S.-N. Li, Y. Jiang, M.-C. Hu and X. Bu, Ultramicroporous Building Units as a Path to Bi-microporous Metal-Organic Frameworks with High Acetylene Storage and Separation Performance, *Angew. Chem., Int. Ed.*, 2019, **58**, 13590–13595.
42 Y.-L. Peng, T. Pham, P. Li, T. Wang, Y. Chen, K.-J. Chen, K. A. Forrest, B. Space, P. Cheng, M. J. Zaworotko and Z. Zhang, Robust Ultramicroporous Metal–Organic Frameworks with Benchmark Affinity for Acetylene, *Angew. Chem., Int. Ed.*, 2018, **57**, 10971–10975.
43 F. Luo, C. Yan, L. Dang, R. Krishna, W. Zhou, H. Wu, X. Dong, Y. Han, T.-L. Hu, M. O'Keeffe, L. Wang, M. Luo, R.-B. Lin and B. Chen, UTSA-74: A MOF-74 Isomer with Two Accessible Binding Sites per Metal Center for Highly Selective Gas Separation, *J. Am. Chem. Soc.*, 2016, **138**, 5678–5684.
44 J. Lee, C. Y. Chuah, J. Kim, Y. Kim, N. Ko, Y. Seo, K. Kim, T. H. Bae and E. Lee, Separation of Acetylene from Carbon Dioxide and Ethylene by a Water-Stable Microporous Metal–Organic Framework with Aligned Imidazolium Groups inside the Channels, *Angew. Chem., Int. Ed.*, 2018, **57**, 7869–7873.
45 R. Liu, Q.-Y. Liu, R. Krishna, W. Wang, C.-T. He and Y.-L. Wang, Water-Stable Europium 1,3,6,8-Tetrakis(4-carboxylphenyl)pyrene Framework for Efficient C_2H_2/CO_2 Separation, *Inorg. Chem.*, 2019, **58**, 5089–5095.
46 Z. Zhang, S. Xian, Q. Xia, H. Wang, Z. Li and J. Li, Enhancement of CO_2 Adsorption and CO_2/N_2 Selectivity on ZIF-8 via Postsynthetic Modification, *AIChE J.*, 2013, **59**, 2195–2206.
47 F. Luo, C. Yan, L. Dang, R. Krishna, W. Zhou, H. Wu, X. Dong, Y. Han, T. L. Hu, M. O'Keeffe, L. Wang, M. Luo, R. B. Lin and B. Chen, UTSA-74: A MOF-74 Isomer with Two Accessible Binding Sites per Metal Center for Highly Selective Gas Separation, *J. Am. Chem. Soc.*, 2016, **138**, 5678–5684.

48 Y. Ye, Z. Ma, R.-B. Lin, R. Krishna, W. Zhou, Q. Lin, Z. Zhang, S. Xiang and B. Chen, Pore Space Partition within a Metal–Organic Framework for Highly Efficient C_2H_2/CO_2 Separation, *J. Am. Chem. Soc.*, 2019, **141**, 4130–4136.

49 H.-M. Wen, C. Liao, L. Li, L. Yang, J. Wang, L. Huang, B. Li, B. Chen and J. Hu, Reversing C_2H_2–CO_2 Adsorption Selectivity in an Ultramicroporous Metal–Organic Framework Platform, *Chem. Commun.*, 2019, **55**, 11354–11357.

50 W. Fan, S. Yuan, W. Wang, L. Feng, X. Liu, X. Zhang, X. Wang, Z. Kang, F. Dai, D. Yuan, D. Sun and H.-C. Zhou, Optimizing Multivariate Metal–Organic Frameworks for Efficient C_2H_2/CO_2 Separation, *J. Am. Chem. Soc.*, 2020, **142**, 8728–8737.

51 Z. H. Rada, H. R. Abid, J. Shang, Y. He, P. Webley, S. Liu, H. Sun and S. Wang, Effects of Amino Functionality on Uptake of CO_2, CH_4 and Selectivity of CO_2/CH_4 on Titanium Based MOFs, *Fuel*, 2015, **160**, 318–327.

52 S. Galli, N. Masciocchi, G. Tagliabue, A. Sironi, J. A. R. Navarro, J. M. Salas, L. Mendez-Liñan, M. Domingo, M. Perez-Mendoza and E. Barea, Polymorphic Coordination Networks Responsive to CO_2, Moisture, and Thermal Stimuli: Porous Cobalt(II) and Zinc(II) Fluoropyrimidinolates, *Chem. – Eur. J.*, 2008, **14**, 9890–9901.

53 R. Ben-Mansour, N. A. A. Qasem and M. A. Habib, Adsorption Characterization and CO_2 Breakthrough of MWCNT/Mg-MOF-74 and MWCNT/MIL-100(Fe) Composites, *Int. J. Energy Environ. Eng.*, 2018, **9**, 169–185.

54 S. Pourebrahimi, M. Kazemeini and L. Vafajoo, Embedding Graphene Nanoplates into MIL-101(Cr) Pores: Synthesis, Characterization, and CO_2 Adsorption Studies, *Ind. Eng. Chem. Res.*, 2017, **56**, 3895–3904.

55 S. Pourebrahimi, M. Kazemeini, E. Ganji Babakhani and A. Taheri, Removal of the CO_2 from Flue Gas Utilizing Hybrid Composite Adsorbent MIL-53(Al)/GNP Metal-Organic Framework, *Microporous Mesoporous Mater.*, 2015, **218**, 144–152.

56 H.-G. Jin, F. Chen, H. Zhang, W. Xu, Y. Wang, J. Fan and Z.-S. Chao, Postmetalation of a New Porphyrin Ligand-Based Metal–Organic Framework for Catalytic Oxidative Carboxylation of Olefins, *J. Mater. Sci.*, 2020, **55**, 16184–16196.